Fission yeast Pdk1 kinase regulates cytokinesis and eisosomes

Madeline L. Chrupcala and James B. Moseley*

Department of Biochemistry and Cell Biology, The Geisel School of Medicine at Dartmouth, Hanover NH

* Address correspondence to: James B. Moseley (james.b.moseley@dartmouth.edu)

Character count (all sections except Materials and Methods and References): 15,616
Running Title: Pdk1 regulates cytokinesis and eisosomes

ABSTRACT
The conserved phosphoinositide-dependent protein kinase PDK1 regulates cell growth and stress signaling in eukaryotes. In the fission yeast *S. pombe*, Pdk1 has been linked to cytokinesis, which could point to new functions for this kinase family. Here, we discovered that Pdk1 localizes to eisosomes, which create invaginations in the plasma membrane, in addition to the spindle pole body (SPB). Pdk1 promotes phosphorylation of the core eisosome protein Pil1 and regulates the length of eisosomes. Dysregulated eisosomes are not responsible for cytokinesis defects previously observed in *pdk1Δ* cells. Instead, we found that Pdk1 regulates localization of the anillin-like protein Mid1 and the protein kinase Sid2, which promotes cytokinesis as part of the septation initiation network (SIN). Our combined results provide insights into the role of Pdk1 in eisosomes and cytokinesis, which extend the functions of this conserved protein kinase family beyond canonical growth control pathways.

INTRODUCTION

Conserved signal transduction pathways coordinate cell growth and division in eukaryotic cells. The phosphoinositide-dependent protein kinase PDK1 functions as a master regulator of cell growth pathways in organisms from yeast through humans (Pearce *et al.*, 2010; Leroux *et al.*, 2018). PDK1 is primarily known for its role in phosphorylating the activation loop of more than 23 downstream AGC family protein kinases in response to growth factor signals. These targets include Akt, PKC, ribosomal S6 kinase, and p70 S6 kinase, with functional connections to cell proliferation, migration, and metabolism (Mora *et al.*, 2004; Bayascas, 2010; Leroux and Biondi, 2023). Given its central role in conserved pathways, PDK1 knockout mice die at embryonic day E9.5 with severe developmental defects (Lawlor *et al.*, 2002). In addition, PDK1 overexpression has been observed in many human cancers and is associated with poor clinical outcomes (Pearn *et al.*, 2007; Eser *et al.*, 2013; Zabkiewicz *et al.*, 2014; Du *et al.*, 2016).

Studies on PDK1-related kinases in diverse organisms has the potential to reveal new functions beyond activation of AGC kinases. The fission yeast *Schizosaccharomyces pombe* expresses two PDK1-related kinases called Ksg1 and Pdk1. *ksg1+* is an essential gene, and the Ksg1 protein appears to activate AGC kinases for functions including meiosis and cell wall biogenesis (Niederberger and Schweingruber, 1999; Gräub *et al.*, 2003; Cipak *et al.*, 2024). The Ksg1 protein has a similar domain layout to human PDK1, including an amino terminal kinase domain and a carboxyl terminal pleckstrin homology (PH) domain, which can interact with lipids (Niederberger and Schweingruber, 1999). In contrast, the *pdk1+* gene is not essential, and Pdk1 has been less studied than its essential counterpart Ksg1. *pdk1Δ* phenotypes include defects in cytokinesis and mitosis (Bimbó *et al.*, 2005; Liu *et al.*, 2021), which might suggest new functions for PDK1-related signaling. The Pdk1 protein sequence includes an amino terminal kinase domain but lacks a PH domain, similar to its budding yeast orthologs Pkh1 and Pkh2 (Casamayor *et al.*, 1999).

In this study, we investigated fission yeast Pdk1 with the goal of learning about new functions. We found that Pdk1 localizes to fission yeast eisosomes, which are invaginations at the plasma membrane, and promotes phosphorylation of the core eisosome protein Pil1 for proper eisosome formation. Septation defects in *pdk1Δ* cells are not due to dysregulated

eisosomes, but rather to delayed assembly of the cytokinetic actomyosin ring. Our findings provide insight into the functions of a conserved protein kinase in a powerful model organism.

RESULTS AND DISCUSSION

Pdk1 regulates eisosomes

As a first step to study Pdk1 function, we examined the localization of Pdk1-mNeonGreen (mNG) in live cells. A previous study on fixed cells reported mitosis-specific localization of Pdk1 to the spindle pole body (SPB) and to a cortical band reminiscent of the assembling cytokinetic actomyosin ring (Bimbó *et al.*, 2005). We observed prominent localization of Pdk1-mNG to the cell cortex in all cells, along with localization to the SPB (Figure 1A). Cortical Pdk1-mNG did not colocalize with Rlc1-mCherry, a marker of the assembling and mature cytokinetic ring (Figure 1B). We conclude that Pdk1 is not a component of the cytokinetic ring precursors, and instead localizes to other structures at the cell cortex.

Cortical Pdk1 forms faint linear structures reminiscent of eisosomes, which are linear invaginations of the plasma membrane formed by the BAR domain protein Pil1 (Kabeche *et al.*, 2011). This possibility is supported by the localization of budding yeast PDK1-related kinases Pkh1 and Pkh2 to eisosomes (Walther *et al.*, 2007). We found that Pdk1-mNG colocalized with Pil1-mCherry (Figure 1C), even though the level of Pdk1-mNG cortical filaments was reduced by the Pil1-mCherry tag. We also found that Pdk1-mNG was absent from the cell cortex in *pil1Δ* cells, which lack eisosomes. In *pil1Δ* cells, Pdk1-mNG localized to the SPB and diffusively in the nucleus and cytoplasm (Figure 1D). These data show that the primary sites of Pdk1 localization in fission yeast cells are the SPB and eisosomes.

We next tested if Pdk1 regulates eisosomes. In budding yeast, conflicting reports have suggested that Pkh1/2 either promote or inhibit eisosome formation (Walther *et al.*, 2007; Luo *et al.*, 2008). We generated a *pdk1Δ* strain that exhibited septation defects consistent with a previous study (Bimbó *et al.*, 2005). We found that Pil1-mCherry filaments were longer in *pdk1Δ* cells compared to wild type (Figure 2A-B). This supports a model where Pdk1 limits eisosome assembly by Pil1. To investigate the underlying mechanism, we tested the possibility that Pdk1 regulates Pil1 phosphorylation. Using Phos-bind SDS-PAGE, which slows the migration of phosphorylated proteins, we observed pronounced smearing of bands for Pil1 in wild type cells (Figure 2C). In contrast, Pil1 collapsed to a single band in *pdk1Δ* cells, showing loss of phosphorylation. Phosphorylated Pil1 was enhanced in *2x-pdk1* cells that express two copies of *pdk1+*. We conclude that Pdk1 promotes Pil1 phosphorylation to limit eisosome assembly. Our combined results show that Pdk1 and Pil1 reciprocally regulate each other: Pil1 promotes Pdk1 localization to eisosomes, and Pdk1 limits the elongation of eisosomes.

Finally, we tested if dysregulated Pil1 causes the septation defect in *pdk1Δ* cells. We found that abnormal septa remained present in *pdk1Δ pil1Δ* cells (Figure 2D), which means that septation defects in *pdk1Δ* cells are not due to excess eisosomes. Therefore, we decided to examine cytokinesis in *pdk1Δ* cells.

Cytokinesis defects in pdk1Δ cells

Fission yeast cytokinesis occurs in 3 defined and reproducible steps. First, cytokinesis proteins assemble at a series of cortical precursor structures called nodes, which are anchored by the anillin-like protein Mid1 and the protein kinase Cdr2 (Paoletti and Chang, 2000; Wu *et al.*,

2006; Almonacid *et al.*, 2009). Nodes condense to form the cytokinetic ring. Second, additional cytokinesis proteins are recruited to the ring in a step termed "maturation" (Wu *et al.*, 2003, 2006; Pollard and Wu, 2010). Third, the cytokinetic ring constricts to separate the two dividing cells. We monitored this process by timelapse microscopy in wild type and *pdk1Δ* cells using Rlc1-mNG to mark the cytokinetic ring and Sad1-mEGFP to mark the SPBs, which provide a temporal clock for assembly and constriction of cytokinetic events (Wu *et al.*, 2003). In wild type cells, the cytokinetic ring assembled, matured, and constricted with expected kinetics. However, the assembly of the cytokinetic ring was significantly slower in *pdk1Δ* cells (Figure 3A-B). Ring maturation and constriction were unaffected in *pdk1Δ* cells (Figure 3C-D). In some *pdk1Δ* cells, cytokinetic rings failed to fully assemble and then fell apart without constricting (Figure 3A). This pattern was observed in approximately 10% of *pdk1Δ* cells. Our results identify ring assembly as a stage of cytokinesis that is defective in *pdk1Δ* cells.

Genetic interactions provided additional support for Pdk1 function in cytokinesis. We observed synthetic genetic defects when *pdk1Δ* was combined with either *cdc15-140* or *rng2-D15* mutations (Supplementary Figure S1). Both Cdc15 and Rng2 make multiple protein-protein interactions within the cytokinetic ring, and Cdc15 also binds directly to lipids (Roberts-Galbraith *et al.*, 2010; Laporte *et al.*, 2011; Padmanabhan *et al.*, 2011; McDonald *et al.*, 2015; Ren *et al.*, 2015). These proteins are essential for cytokinetic ring formation and cell viability, and the *cdc15-140* and *rng2-D15* mutations are temperature-sensitive (Nurse *et al.*, 1976; Fankhauser *et al.*, 1995; Eng *et al.*, 1998). We found reduced growth and increased septation defects for *pdk1Δ cdc15-140* and *pdk1Δ rng2-D15* double mutants, when compared to the single mutants (Supplementary Figure S1A-C). These results reinforce the functional importance of Pdk1 in cytokinesis.

To gain mechanistic insight into cytokinesis defects in *pdk1Δ* cells, we examined the localization of key cytokinesis proteins in these mutant cells. The cytokinetic ring assembles from precursor nodes, which are positioned by Cdr2 and Mid1. We did not observe defects in the distribution of Cdr2 nodes in *pdk1Δ* cells (Figure 4A). This result was confirmed by measuring the distance of cell length containing Cdr2 nodes, which was similar in wild type and *pdk1Δ* cells (Figure 4B). However, we found that Mid1 cortical nodes were more spread out in *pdk1Δ* cells compared to wild type cells (Figure 4C-D). This suggests that disorganization of cortical Mid1 nodes might contribute to delayed cytokinetic ring assembly in *pdk1Δ* cells. We also tested if cytokinetic rings in *pdk1Δ* have altered levels of key proteins, but we did not observe changes in the levels of myosin proteins Rlc1, Myp2, and Myo2, formin Cdc12, or Rho-GAP Rga7 at the cytokinetic rings of *pdk1Δ* cells (Supplementary Figure S2).

Finally, because cytokinetic rings failed to constrict in some *pdk1Δ* cells, we tested if Pdk1 contributes to cytokinesis by promoting signaling by the septation initiation network (SIN). The SIN pathway initiates cytokinetic ring constriction through the regulated activation and localization of Sid2 kinase to the cytokinetic ring (Simanis, 2015). We tested the timing of Sid2-GFP recruitment to the cytokinetic ring using SPB separation to normalize cytokinesis events between cells. We also tracked the cytokinetic ring marker Rlc1-mCherry in these same cells. Interestingly, we did not observe differences in the recruitment of Sid2 or Rlc1 when comparing wild type and *pdk1Δ* cells that completed cytokinesis (Figure 5A-C). Both the timing and levels of recruitment were unaffected. However, approximately 20% of *pdk1Δ* cells (4 out of 21) did not recruit Sid2 to the cytokinetic ring and subsequently failed cytokinesis (Figure 5A). In these

pdk1Δ cells, Rlc1-mCherry formed a cytokinetic ring, but it did not initiate constriction and the cells did not complete cytokinesis. This failure to recruit Sid2 was not seen in any wild type cells (0 out of 21). We conclude that SIN signaling fails in a subset of *pdk1Δ* cells, leading to binucleated cells and defects in later division events.

Conclusions

We have identified new localization and functions for the conserved protein kinase Pdk1 in fission yeast. We found that Pdk1 localizes to and regulates cortical eisosomes, likely through phosphorylation of the core eisosome protein Pil1. Budding yeast Pdk1-related proteins play a similar role, but their function at eisosomes has been debated (Walther *et al.*, 2007; Luo *et al.*, 2008). Our results support a model where Pdk1 phosphorylates Pil1 to limit eisosome growth or stability. Future work will be needed to test this model *in vitro* with purified proteins. We also found that cytokinesis defects in *pdk1Δ* cells originate from abnormal spread of Mid1 nodes and failure to recruit Sid2. We did not observe localization of Pdk1 to cytokinetic nodes or the cytokinetic ring. Instead, it seems likely that Pdk1 activity at the SPB contributes to these cytokinesis-related events. In addition to linking Pdk1 with eisosomes and cytokinesis events, our results identify proteins that might be confirmed as Pdk1 substrates in future work. We note that many substrates of PDK-related kinases have a PDK1-interacting fragment (PIF), defined by the sequence motif F-X-X-F/Y-S/T/D-F/Y (Balendran *et al.*, 1999; Biondi *et al.*, 2000). We identified a PIF motif in Sid2 as well as the SIN protein Cut11. Both Sid2 and Cut11 localize at the SPB like Pdk1. We also found PIFs in the cytokinesis proteins Myp2 and Rga7. Future work on these proteins might define the molecular links between Pdk1 and cytokinesis. More generally, continued work on the role of Pdk1 in fission yeast cytokinesis has the potential to define the broad roles of PDK family kinases in eukaryotic cell growth and division.

MATERIALS AND METHODS

Strain construction and growth

Standard *Schizosaccharomyces pombe* media and methods were used (Moreno *et al.*, 1991). Strains used in this study are listed in Supplementary Table S1. Gene deletions and tagging were performed using PCR and homologous recombination (Bähler *et al.*, 1998).

pDC99-PPdk1-Pdk1-mNeonGreen-Tadh1 was generated by Gibson assembly using PCR products. The Ppdk1-mNeonGreen insert was amplified from genomic DNA from JM8217 (*pdk1-mNeonGreen::hphR*). The pDC99 backbone was amplified from pJM1512 (*pDC99-Parf6-Arf6-mRuby-Tadh1*). The resulting plasmid was linearized by PCR and integrated into the *leu1* locus of JM737 (*ura4-D18*). Correct colonies were those that grew on EMM-Uri medium but not on EMM-Leu medium. The resulting strain was crossed to JM8289 (*pdk1Δ::kanR ura4-D18 leu+*) to eliminate the copy at the endogenous *pdk1* locus.

In Supplementary Figure S1, double mutants were constructed by crossing JM8220 (*pdk1Δ*::kanMX6) to known cytokinetic mutants, including *rng2-D5* and *cdc15-140*. In Supplementary Figure S1A, cells were spotted by 10-fold serial dilutions on YE4S plates and incubated at 25°C, 30°C, 32°C, or 34°C for three days before imaging. Cells were grown in YE4S at 25°C before being stained with Blankophor to mark the cell wall in Supplementary Figure S1B.

Microscopy and Image Analysis

All imaging was done at room temperature using a Nikon Eclipse Ti-2E microscope with a Yokogawa CSU-WI spinning disk confocal system. This system was equipped with a Photometrics Prime BSI sCMOS camera and a 100x 1.45-NA CFI Plan Apochromat Lambda objective. Cells were grown in YE4S at 25°C unless otherwise stated.

All image analysis was performed in ImageJ (Schneider *et al.*, 2012). All statistics and graphs were generated using Prism10 (GraphPad software).

All strains imaged in Figure 1 were grown in in YE4S (yeast extract with 4 supplements) at 25°C. In Figure 1A (left), Z stacks were obtained by acquiring 13 slices with a 0.5µm step size through the entire cell. mNG images are maximum intensity projections with inverted fluorescence. In Figure 1A (right), single middle focal planes and maximum intensity projections are shown of a single cell expressing Pdk1-mNeonGreen. Wild type cells expressing Pdk1-mNeonGreen, Rlc1-mCherry to mark the cytokinetic ring, and Sad1-mCherry to label the Spindle Pole Body (SPB) were imaged under glass coverslips in Figure 1B. Z stacks were obtained by acquiring 13 slices with a 0.5µm step size through the entire cell. mCh and mNG images are maximum intensity projections through the top half of the cell. Merged images are maximum intensity projections of mCh (magenta) and mNG (cyan) channels overlaid. In Figure 1C, wild type cells expressing Pdk1-mNeonGreen and Pil1-mCherry to mark eisosomes were imaged under glass coverslips. Z stacks were obtained by acquiring 13 slices with a 0.5µm step size through the entire cell. mCh and mNG images are maximum intensity projections with inverted fluorescence. Merged images are maximum intensity projections of mCh (magenta) and mNG (cyan) channels overlaid. Representative wild type and *pil1Δ* cells expressing Pdk1-mNeonGreen were imaged under glass coverslips in Figure 1D. Z stacks were obtained by acquiring 13 slices with a 0.5µm step size through the entire cell. Left panel, mNG images are maximum intensity projections with inverted fluorescence. Right panel, single middle focal planes and maximum intensity projections for a single wild type and *pil1Δ* cell expressing Pdk1-mNeonGreen. All brightfield images represent a single middle focal plane.

Wild type and *pdk1Δ* cells expressing Pil1-mCherry were grown in YE4S at 25°C in Figure 2A. The cells were maintained in rich media for 48 hours prior to being imaged under glass coverslips. In Figure 2A, Z stacks were obtained by acquiring 13 slices with a 0.5µm step size through the entire cell. mCh images are maximum intensity projections with inverted fluorescence. Brightfield images are single middle focal planes. To measure eisosome length in Figure 2B, maximum intensity projections through the top half of the cell were generated. Individual Pil1-mCherry filaments were measured using the straight-line tool in Image J. At least 235 Pil1-mCherry filaments were measured for each strain examined. A Welch's unpaired t-test was used to compare the two strains. Prior to being stained with Blankophor to mark the cell wall, the strains in Figure 2D were grown in YE4S at 25°C for 48 hours. Single middle focal plane images with inverted fluorescence are shown in Figure 2D.

In Figure 3A, wild type and *pdk1*Δ cells expressing Rlc1-mNeonGreen to mark the CAR and Sad1-meGFP to label the SPB were imaged on YE4S agarose pads. Representative sum projections with inverted fluorescence are shown. Brightfield images correspond to the first time point captured. Images were captured in 5-minute intervals. Z stacks were obtained by acquiring 7 slices with a 0.5 µm step size through half the cell. The onset of mitosis was

monitored by Sad1-meGFP signal (Nabeshima *et al.*, 1998). In Figure 3B, ring assembly was defined as the time taken to form an intact cytokinetic ring from the onset of mitosis. In Figure 3C, ring maturation was reported as the period between cytokinetic ring formation and the onset of ring constriction. In Figure 3D, ring constriction was described as the time from the initiation of ring constriction to the disappearance of Rlc1-mNeonGreen from the division site. At least 30 cells were analyzed for each strain in Figure 3. Welch's unpaired t-tests were used to compare wild type and *pdk1*Δ cells in Figure 3.

In Figure 4A and Figure 4C, wild type and *pdk1*Δ cells expressing (A) Cdr2-meGFP and (B) Mid1-mNeonGreen were grown in YE4S at 25°C for 48 hours. Cells were imaged in YE4S and mounted under glass coverslips. Z stacks were obtained by acquiring 13 slices with 0.5 µm step size through the entire cell. Brightfield images are a single middle focal plane. mEGFP and mNG images are maximum intensity projections with inverted fluorescence. To determine the average node distance of Cdr2-mEGFP (Figure 4B) and Mid1-mNeonGreen (Figure 4D), a maximum intensity projection through the top half of the cell was generated and the length of the medial node domain was measured for both sides of the cell. The resulting values were averaged and plotted against the length of the cell examined. For Figures 4B and 4D, at least 100 cells were analyzed for each strain. All statistical tests performed in this figure are Welch's unpaired t-tests. NS indicates p value > 0.05; * indicates p value < 0.05.

In Figure 5, wild type and *pdk1Δ* cells expressing Sid2-GFP and Rlc1-mCherry were imaged on YE4S agarose pads in 5-minute intervals. Z stacks were obtained by acquiring 7 slices with a 0.5µm step size through half the cell. The onset of mitosis was monitored by Spindle Pole Body separation using Sid2-GFP signal (Nabeshima *et al.*, 1998). In Figure 5A, brightfield images are a single middle focal plane corresponding to the first time point analyzed. GFP and mCh images are sum projections with inverted fluorescence. To determine the fluorescence intensity of Sid2-GFP and Rlc1-mCherry at the cytokinetic ring, an ROI was drawn around the ring using the rectangular tool in ImageJ. This ROI was used to measure the integrated density from sum intensity projections. The same ROI was moved to a neighboring region without any cells to measure the integrated density of the background. This value was used to subtract background signal. This process was repeated at all time points examined. The mean fluorescence intensity of Sid2-GFP (Figure 5B) and Rlc1-mCherry (Figure 5C) were plotted against time since Spindle Pole Body separation. Error bars correspond to the standard deviation. At least 10 cells were analyzed for each strain in Figures 5B and 5C.

To determine the fluorescence intensity of different cytokinetic ring proteins in wild type and *pdk1*Δ cells, cells were grown in YE4S at 25°C for 48 hours. Cells were imaged in YE4S and mounted under glass coverslips. Z stacks were obtained by acquiring 13 slices with 0.5 µm step size through the entire cell. The rectangular tool in ImageJ was used to draw an ROI around the cytokinetic ring. This ROI was used to measure the integrated density from sum intensity projections. The same ROI was moved to a neighboring region without any cells to measure the integrated density. This value was used to subtract background signal. At least 25 cells were analyzed for each strain in Supplementary Figure S2. All statistical analyses performed in Supplementary Figure S2 were Welch's unpaired t-tests.

Western blots

Fission yeast whole cell lysates were prepared by growing cells in YE4S to mid-logarithmic phase. Two OD_{600} samples were harvested and rapidly frozen in liquid nitrogen. Cell pellets were resuspended in sample buffer (15% glycerol, 4.5% SDS, 97.5mM Tris pH6.8, 10% 2-mercaptoethanol, 50mM β-glycerophosphate, 50mM sodium fluoride, 5mM sodium orthovanadate, 1x EDTA-free protease inhibitor cocktail (Sigma Aldrich). The samples were lysed with acid-washed glass beads (Sigma Aldrich) in a Mini-BeadBeater-16 (BioSpec, Bartlesville, OK) for 2 minutes at 4°C. Following this, cell lysates were incubated at 99°C for 5 minutes. Cell lysates were briefly centrifuged, and the supernatant was isolated as the clarified lysate. 8.0% acrylamide gels were poured containing 50µM Phosbind acrylamide (APExBIO Catalog No. F4002) and 100µM $MnCl_2$. 5µl of the cell lysates were separated by SDS-PAGE at 20mAmps. Gels were washed once in transfer buffer containing 10mM EDTA for 10 minutes. Next, gels were washed twice in transfer buffer without EDTA for 10 minutes. Blots were transferred to a nitrocellulose membrane using the Trans-blot Turbo Transfer System (Bio-Rad). Blots were first probed with custom anti-Pil1 primary antibodies at 4°C. Blots were washed in 1X TBST and then probed with goat anti-rabbit secondary antibody (LI-COR Lot No. C50331-05). Before being developed on a LiCor Odyssey CLx, blots were washed multiple times in 1X TBST and once in 1X TBS.

ACKNOWLEDGEMENTS

We thank members of the Moseley lab for helpful discussions. This work was supported by a grant from the National Institutes of General Medical Sciences to J.B.M. (R35GM149248). This work was also supported by bioMT through NIH NIGMS grant P20GM113132.

REFERENCES

Almonacid, M, Moseley, JB, Janvore, J, Mayeux, A, Fraisier, V, Nurse, P, and Paoletti, A (2009). Spatial control of cytokinesis by Cdr2 kinase and Mid1/anillin nuclear export. Curr Biol 19, 961–966.

Bähler, J, Wu, JQ, Longtine, MS, Shah, NG, McKenzie, A, Steever, AB, Wach, A, Philippsen, P, and Pringle, JR (1998). Heterologous modules for efficient and versatile PCR-based gene targeting in Schizosaccharomyces pombe. Yeast 14, 943–951.

Balendran, A, Casamayor, A, Deak, M, Paterson, A, Gaffney, P, Currie, R, Downes, CP, and Alessi, DR (1999). PDK1 acquires PDK2 activity in the presence of a synthetic peptide derived from the carboxyl terminus of PRK2. Curr Biol 9, 393–404.

Bayascas, JR (2010). PDK1: the major transducer of PI 3-kinase actions. Curr Top Microbiol Immunol 346, 9–29.

Bimbó, A, Liu, J, and Balasubramanian, MK (2005). Roles of Pdk1p, a fission yeast protein related to phosphoinositide-dependent protein kinase, in the regulation of mitosis and cytokinesis. Mol Biol Cell 16, 3162–3175.

Biondi, RM, Cheung, PC, Casamayor, A, Deak, M, Currie, RA, and Alessi, DR (2000). Identification of a pocket in the PDK1 kinase domain that interacts with PIF and the C-terminal residues of PKA. EMBO J 19, 979–988.

Casamayor, A, Torrance, PD, Kobayashi, T, Thorner, J, and Alessi, DR (1999). Functional counterparts of mammalian protein kinases PDK1 and SGK in budding yeast. Curr Biol 9, 186–197.

Cipak, L, Sivakova, B, Bellova, J, Danchenko, M, Jurcik, J, Cipakova, I, Lalakova, LO, Gregan, J, and Barath, P (2024). Characterization of Ksg1 protein kinase-dependent phosphoproteome in the fission yeast S. pombe. Biochem Biophys Res Commun 736, 150895.

Du, J, Yang, M, Chen, S, Li, D, Chang, Z, and Dong, Z (2016). PDK1 promotes tumor growth and metastasis in a spontaneous breast cancer model. Oncogene 35, 3314–3323.

Eng, K, Naqvi, NI, Wong, KC, and Balasubramanian, MK (1998). Rng2p, a protein required for cytokinesis in fission yeast, is a component of the actomyosin ring and the spindle pole body. Curr Biol 8, 611–621.

Eser, S, Reiff, N, Messer, M, Seidler, B, Gottschalk, K, Dobler, M, Hieber, M, Arbeiter, A, Klein, S, Kong, B, *et al.* (2013). Selective requirement of PI3K/PDK1 signaling for Kras oncogene-driven pancreatic cell plasticity and cancer. Cancer Cell 23, 406–420.

Fankhauser, C, Reymond, A, Cerutti, L, Utzig, S, Hofmann, K, and Simanis, V (1995). The S. pombe cdc15 gene is a key element in the reorganization of F-actin at mitosis. Cell 82, 435–444.

Gräub, R, Hilti, N, Niederberger, C, and Schweingruber, ME (2003). Ksg1, a homologue of the phosphoinositide-dependent protein kinase 1, controls cell wall integrity in Schizosaccharomyces pombe. J Basic Microbiol 43, 473–482.

Kabeche, R, Baldissard, S, Hammond, J, Howard, L, and Moseley, JB (2011). The filament-forming protein Pil1 assembles linear eisosomes in fission yeast. Molecular Biology of the Cell 22, 4059–4067.

Laporte, D, Coffman, VC, Lee, I-J, and Wu, J-Q (2011). Assembly and architecture of precursor nodes during fission yeast cytokinesis. J Cell Biol 192, 1005–1021.

Lawlor, MA, Mora, A, Ashby, PR, Williams, MR, Murray-Tait, V, Malone, L, Prescott, AR, Lucocq, JM, and Alessi, DR (2002). Essential role of PDK1 in regulating cell size and development in mice. EMBO J 21, 3728–3738.

Leroux, AE, and Biondi, RM (2023). The choreography of protein kinase PDK1 and its diverse substrate dance partners. Biochem J 480, 1503–1532.

Leroux, AE, Schulze, JO, and Biondi, RM (2018). AGC kinases, mechanisms of regulation and innovative drug development. Semin Cancer Biol 48, 1–17.

Liu, K, Liu, Q, Sun, Y, Fan, J, Zhang, Y, Sakamoto, N, Kuno, T, and Fang, Y (2021). Phosphoinositide-Dependent Protein Kinases Regulate Cell Cycle Progression Through the SAD Kinase Cdr2 in Fission Yeast. Front Microbiol 12, 807148.

Luo, G, Gruhler, A, Liu, Y, Jensen, ON, and Dickson, RC (2008). The sphingolipid long-chain base-Pkh1/2-Ypk1/2 signaling pathway regulates eisosome assembly and turnover. J Biol Chem 283, 10433–10444.

McDonald, NA, Vander Kooi, CW, Ohi, MD, and Gould, KL (2015). Oligomerization but Not Membrane Bending Underlies the Function of Certain F-BAR Proteins in Cell Motility and Cytokinesis. Developmental Cell 35, 725–736.

Mora, A, Komander, D, van Aalten, DMF, and Alessi, DR (2004). PDK1, the master regulator of AGC kinase signal transduction. Semin Cell Dev Biol 15, 161–170.

Moreno, S, Klar, A, and Nurse, P (1991). Molecular genetic analysis of fission yeast Schizosaccharomyces pombe. Meth Enzymol 194, 795–823.

Nabeshima, K, Nakagawa, T, Straight, AF, Murray, A, Chikashige, Y, Yamashita, YM, Hiraoka, Y, and Yanagida, M (1998). Dynamics of centromeres during metaphase-anaphase transition in fission yeast: Dis1 is implicated in force balance in metaphase bipolar spindle. Mol Biol Cell 9, 3211–3225.

Niederberger, C, and Schweingruber, ME (1999). A Schizosaccharomyces pombe gene, ksg1, that shows structural homology to the human phosphoinositide-dependent protein kinase PDK1, is essential for growth, mating and sporulation. Mol Gen Genet 261, 177–183.

Nurse, P, Thuriaux, P, and Nasmyth, K (1976). Genetic control of the cell division cycle in the fission yeast Schizosaccharomyces pombe. Mol Gen Genet 146, 167–178.

Padmanabhan, A, Bakka, K, Sevugan, M, Naqvi, NI, D'souza, V, Tang, X, Mishra, M, and Balasubramanian, MK (2011). IQGAP-related Rng2p organizes cortical nodes and ensures position of cell division in fission yeast. Curr Biol 21, 467–472.

Paoletti, A, and Chang, F (2000). Analysis of mid1p, a protein required for placement of the cell division site, reveals a link between the nucleus and the cell surface in fission yeast. Mol Biol Cell 11, 2757–2773.

Pearce, LR, Komander, D, and Alessi, DR (2010). The nuts and bolts of AGC protein kinases. Nat Rev Mol Cell Biol 11, 9–22.

Pearn, L, Fisher, J, Burnett, AK, and Darley, RL (2007). The role of PKC and PDK1 in monocyte lineage specification by Ras. Blood 109, 4461–4469.

Pollard, TD, and Wu, J-Q (2010). Understanding cytokinesis: lessons from fission yeast. Nat Rev Mol Cell Biol 11, 149–155.

Ren, L, Willet, AH, Roberts-Galbraith, RH, McDonald, NA, Feoktistova, A, Chen, J-S, Huang, H, Guillen, R, Boone, C, Sidhu, SS, *et al.* (2015). The Cdc15 and Imp2 SH3 domains cooperatively scaffold a network of proteins that redundantly ensure efficient cell division in fission yeast. Mol Biol Cell 26, 256–269.

Roberts-Galbraith, RH, Ohi, MD, Ballif, BA, Chen, J-S, McLeod, I, McDonald, WH, Gygi, SP, Yates, JR, and Gould, KL (2010). Dephosphorylation of F-BAR protein Cdc15 modulates its conformation and stimulates its scaffolding activity at the cell division site. Mol Cell 39, 86–99.

Schneider, CA, Rasband, WS, and Eliceiri, KW (2012). NIH Image to ImageJ: 25 years of image analysis. Nat Methods 9, 671–675.

Simanis, V (2015). Pombe's thirteen - control of fission yeast cell division by the septation initiation network. Journal of Cell Science 128, 1465–1474.

Walther, TC, Aguilar, PS, Fröhlich, F, Chu, F, Moreira, K, Burlingame, AL, and Walter, P (2007). Pkh-kinases control eisosome assembly and organization. EMBO J 26, 4946–4955.

Wu, J-Q, Kuhn, JR, Kovar, DR, and Pollard, TD (2003). Spatial and temporal pathway for assembly and constriction of the contractile ring in fission yeast cytokinesis. Dev Cell 5, 723–734.

Wu, J-Q, Sirotkin, V, Kovar, DR, Lord, M, Beltzner, CC, Kuhn, JR, and Pollard, TD (2006). Assembly of the cytokinetic contractile ring from a broad band of nodes in fission yeast. J Cell Biol 174, 391–402.

Zabkiewicz, J, Pearn, L, Hills, RK, Morgan, RG, Tonks, A, Burnett, AK, and Darley, RL (2014). The PDK1 master kinase is over-expressed in acute myeloid leukemia and promotes PKC-mediated survival of leukemic blasts. Haematologica 99, 858–864.

FIGURE LEGENDS

Figure 1. Pdk1 localizes to eisosomes. (A) Representative images of cells expressing Pdk1-mNG. Left, mNG images are maximum intensity projections with inverted fluorescence. Scale bar, 7µm. Right, single focal planes and maximum intensity projection for a single cell. (B) Representative images of cells expressing Pdk1-mNG, Rlc1-mCherry to mark the cytokinetic ring, and Sad1-mCherry to label the Spindle Pole Body (SPB). mNG and mCh images are maximum intensity projections through the top half of the cell. Merged images are maximum intensity projections of mNG (cyan) and mCh (magenta) channels overlaid. Scale bar, 5µm. (C) Representative images of cells expressing Pdk1-mNG and Pil1-mCherry to mark eisosomes. mCh and mNG images are maximum intensity projections with inverted fluorescence. Merged images are maximum intensity projections of mCh (magenta) and mNG (cyan) channels overlaid. Yellow boxed region is expanded at bottom. Scale bar, 7µm. (D) Left, representative images of wild type and *pil1Δ* cells expressing Pdk1-mNG. mNG images are maximum intensity projections with inverted fluorescence. Scale bar, 7µm. Right, single focal planes and maximum intensity projection for a single wild type or *pil1Δ* cell expressing Pdk1-mNG.

Figure 2. Pdk1 regulates eisosomes and promotes phosphorylation of Pil1 (A) Representative images of wild type and *pdk1Δ* cells expressing Pil1-mCherry. mCh images are maximum intensity projections with inverted fluorescence. Scale bar, 14µm. (B) Quantification of Pil1-mCherry eisosome length in wild type and *pdk1Δ* cells. >235 cells were analyzed for each strain. Welch's unpaired t-test was used to compare the two strains. **** indicates a p value < 0.0001. (C) Western blot analysis of Pil1 phosphorylation status in whole-cell lysates from *pil1Δ*, wild type, *pdk1Δ*, and *2x-pdk1* cells. (D) Representative images of cells stained with Blankophor to mark the cell wall for the indicated strains. Blankophor images are a single middle focal plane with inverted fluorescence. Scale bar, 14µm.

Figure 3. Loss of Pdk1 slows assembly of the cytokinetic actomyosin ring. (A) Representative time-lapse montage of wild type and *pdk1*Δ cells expressing Rlc1-mNG to mark the CAR and Sad1-meGFP to label the SPB. Images were captured in 5-minute intervals. Scale bar, 7µm. (B-D) Duration of ring assembly (B), ring maturation (C), and ring constriction (D) in wild type and *pdk1*Δ cells. N ≥ 30 cells each. All statistical tests in this figure are Welch's unpaired t-tests. **** indicates p value < 0.0001, ns indicates p value > 0.05.

Figure 4. Disorganization of Mid1 cortical localization in *pdk1Δ* cells. (A) Representative images of wild type and *pdk1Δ* cells expressing Cdr2-mEGFP. mEGFP images are maximum intensity projections through the top half of the cell with inverted fluorescence. Scale bar, 14µm. (B) Quantification of average Cdr2-mEGFP node distance versus cell size in wild type and *pdk1*Δ cells. Error bars correspond to minimum and maximum average node distance for each cell size bin. At least 100 cells were analyzed for each condition. (C) Representative images of wild type and *pdk1*Δ cells expressing Mid1-mNG. mNG images are maximum intensity projections through the top half of the cell with inverted fluorescence. Scale bar, 7µm. (D) Quantification of average Mid1-mNeonGreen node distance versus cell size in wild type and *pdk1Δ* cells. Error bars correspond to minimum and maximum average node distance for each cell size bin. At least 100

cells were analyzed for each condition. All statistical tests performed in this figure are Welch's unpaired t-tests. NS indicates *p* value > 0.05; * indicates *p* value < 0.05.

Figure 5. Localization of Sid2 kinase to the division site in *pdk1Δ* cells. (A) Time-lapse montage of wild type and *pdk1Δ* cells expressing Sid2-GFP and Rlc1-mCherry to mark the cytokinetic ring. Images are captured in 5-minute intervals. GFP and mCh images are sum projections of representative cells with inverted fluorescence. Brightfield images are single middle focal planes from the first time point shown. Scale bar, 5µm. (B) Quantification of Sid2-GFP recruitment to the cytokinetic ring in wild type and *pdk1Δ* cells. Time corresponds to minutes since Spindle Pole Body (SPB) separation, as determined by Sid2-GFP signal. N ≥ 10 cells each. Errors bars indicate mean and error ± standard deviation. (C) Quantification of Rlc1-mCh recruitment to the cytokinetic ring in wild type and *pdk1Δ* cells. Time corresponds to minutes since Spindle Pole Body (SPB) separation, as determined by Sid2-GFP signal. N ≥ 10 cells each. Errors bars indicate mean and error ± standard deviation.

Supplementary Figure 1. Genetic interactions between *pdk1Δ* and cytokinesis mutants. (A) Serial-dilution growth assays for each indicated strain at 25°, 30°, 32°, and 34°C. (B) Representative images of cells stained with Blankophor to mark the cell wall for the indicated strains. Images are a single middle focal plane with inverted fluorescence. Cells were grown at 25°. Scale bar, 14µm. (C) Quantification of septation index for the indicated strains.

Supplementary Figure 2. Quantification of the fluorescence intensity of the indicated proteins at the cytokinetic ring in wild type and *pdk1Δ* cells. NS indicates *p* value > 0.05; * indicates *p* value < 0.05; ** indicates *p* value < 0.005. All statistical tests performed in this figure are Welch's unpaired t-tests.

Figure 1.

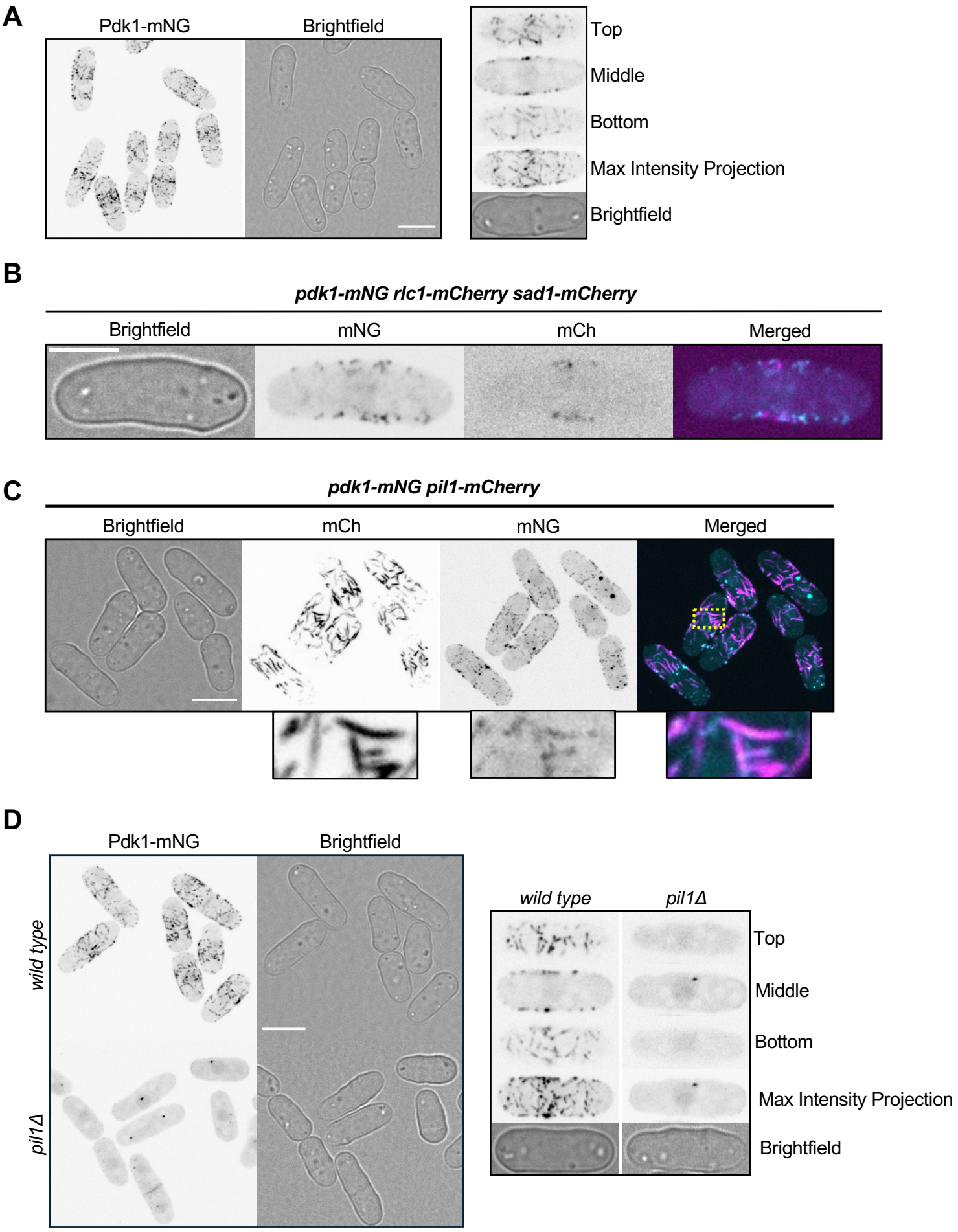
A
Pdk1-mNG
Brightfield
Top
Middle
Bottom
Max Intensity Projection
Brightfield
B
pdk1-mNG rlc1-mCherry sad1-mCherry
Brightfield
mNG
mCh
Merged
C
pdk1-mNG pil1-mCherry
Brightfield
mCh
mNG
Merged
D
Pdk1-mNG
Brightfield
wild type
pil1Δ
wild type
pil1Δ
Top
Middle
Bottom
Max Intensity Projection
Brightfield

Figure 2.

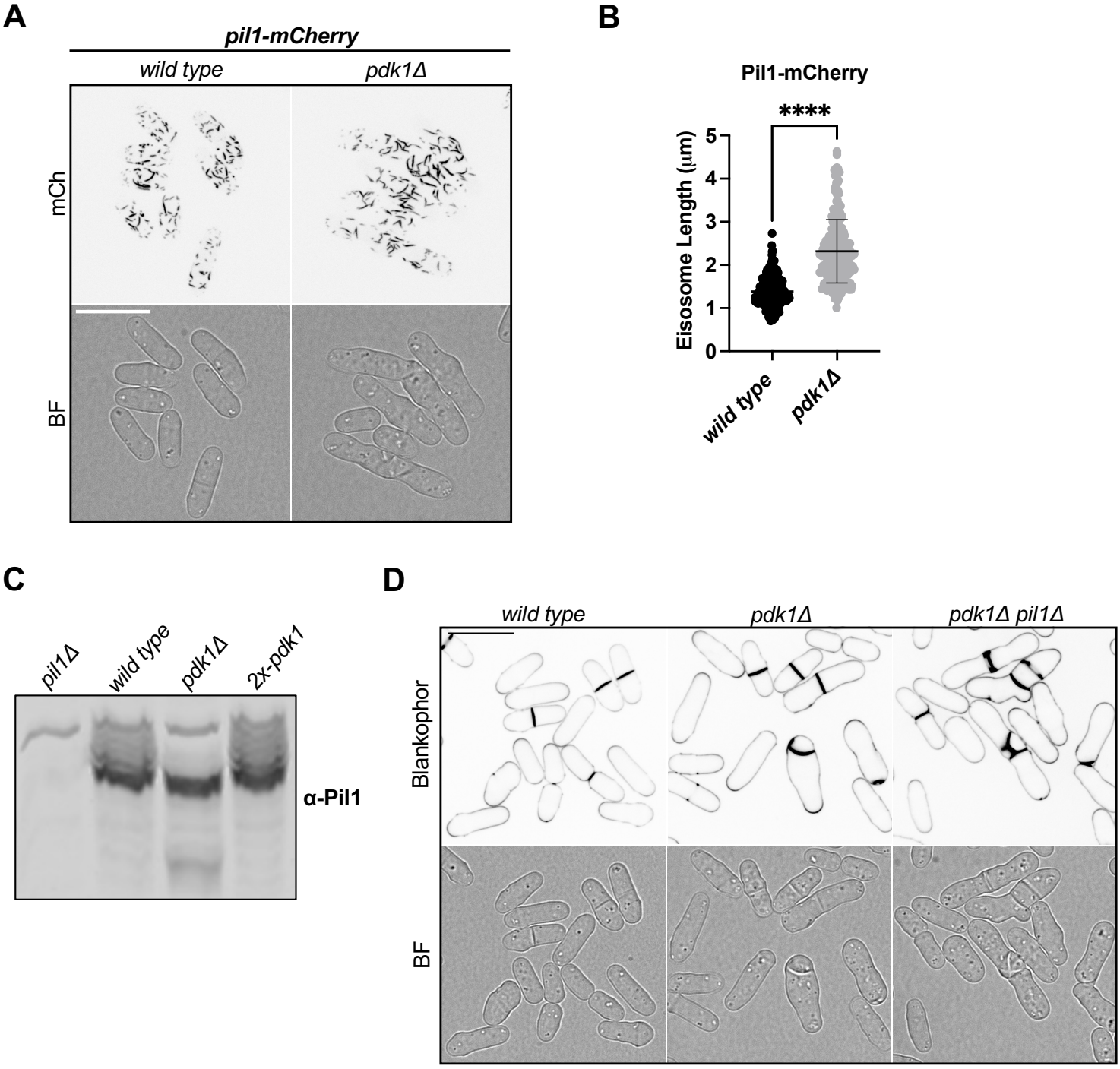
A
pil1-mCherry
wild type
pdk1Δ
mCh
BF
B
Pil1-mCherry
****
Eisosome Length (μm)
0
1
2
3
4
5
wild type
pdk1Δ
C
pil1Δ
wild type
pdk1Δ
2x-pdk1
α-Pil1
D
wild type
pdk1Δ
pdk1Δ pil1Δ
Blankophor
BF

Figure 3.

A

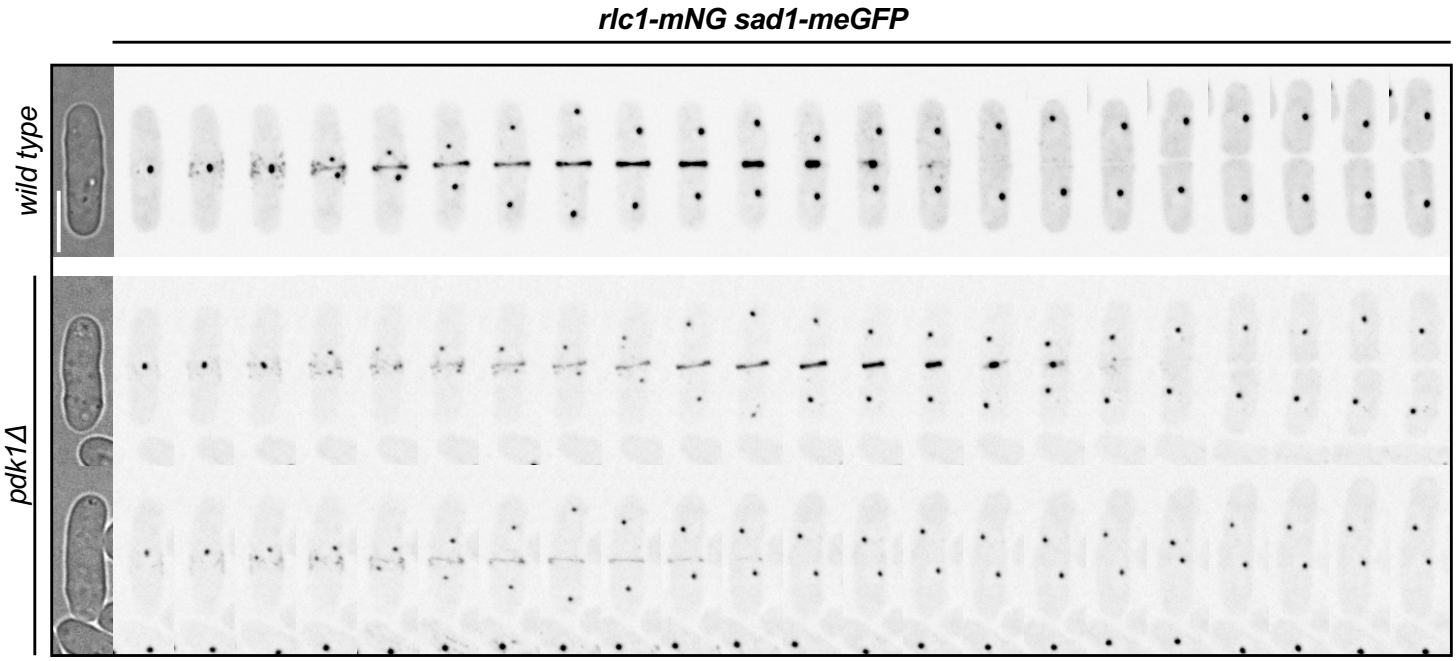

B

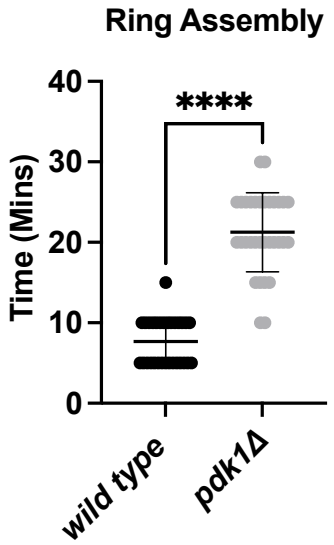

C

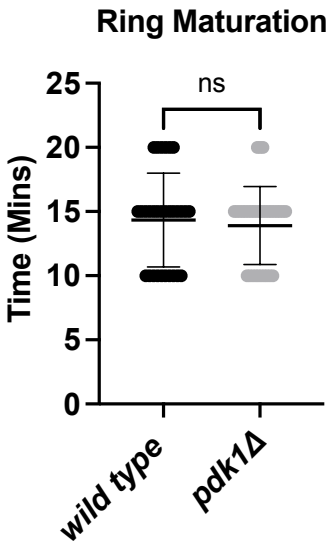

D

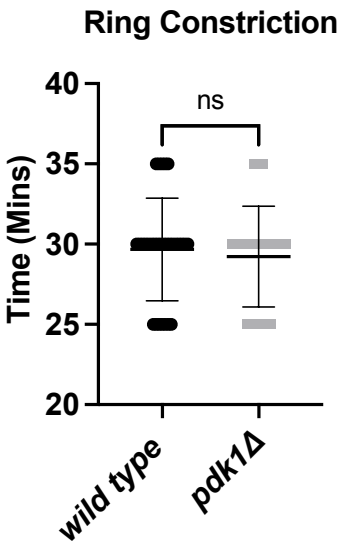

Figure 4.

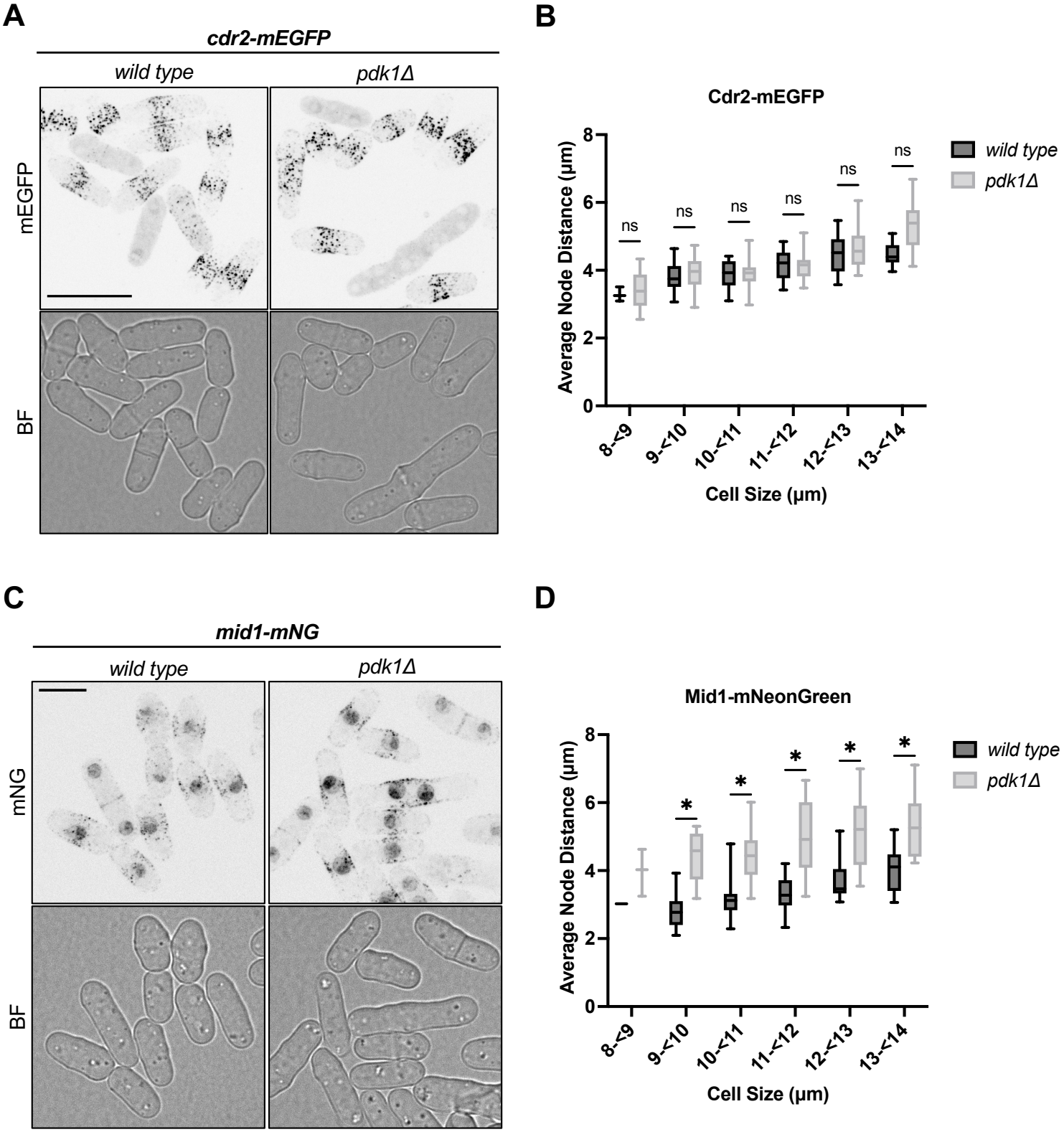
A
cdr2-mEGFP
wild type
pdk1Δ
mEGFP
BF
B
Cdr2-mEGFP
Average Node Distance (µm)
Cell Size (µm)
8-<9
9-<10
10-<11
11-<12
12-<13
13-<14
ns
wild type
pdk1Δ
C
mid1-mNG
wild type
pdk1Δ
mNG
BF
D
Mid1-mNeonGreen
Average Node Distance (µm)
Cell Size (µm)
8-<9
9-<10
10-<11
11-<12
12-<13
13-<14
*
wild type
pdk1Δ

Figure 5.

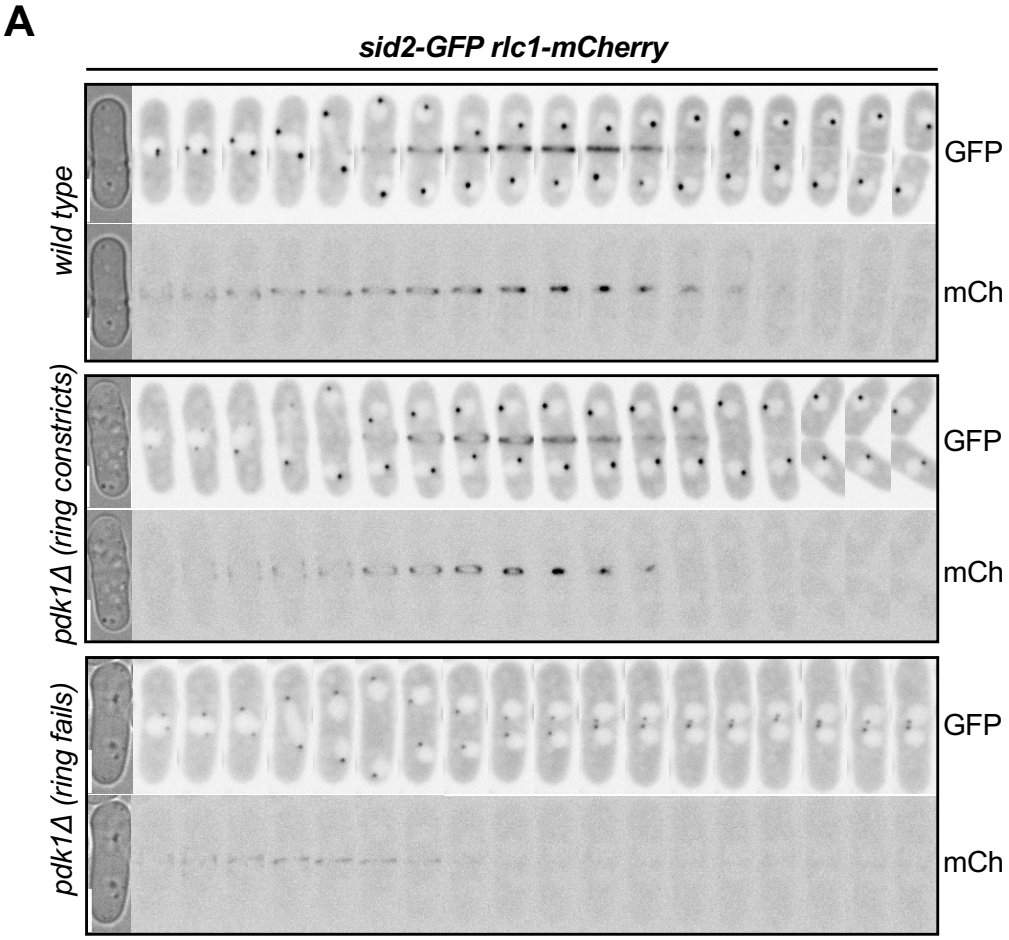
A
sid2-GFP rlc1-mCherry
wild type
pdk1Δ (ring constricts)
pdk1Δ (ring fails)
GFP
mCh

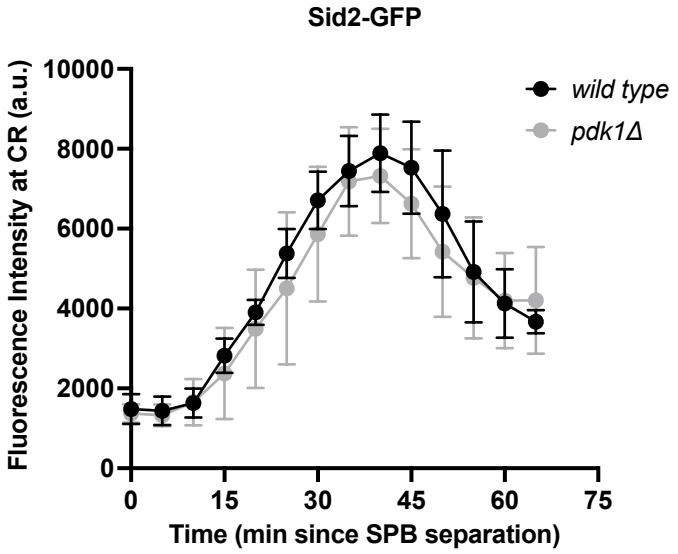
B
Sid2-GFP
Fluorescence Intensity at CR (a.u.)
Time (min since SPB separation)
wild type
pdk1Δ
0
2000
4000
6000
8000
10000
0
15
30
45
60
75

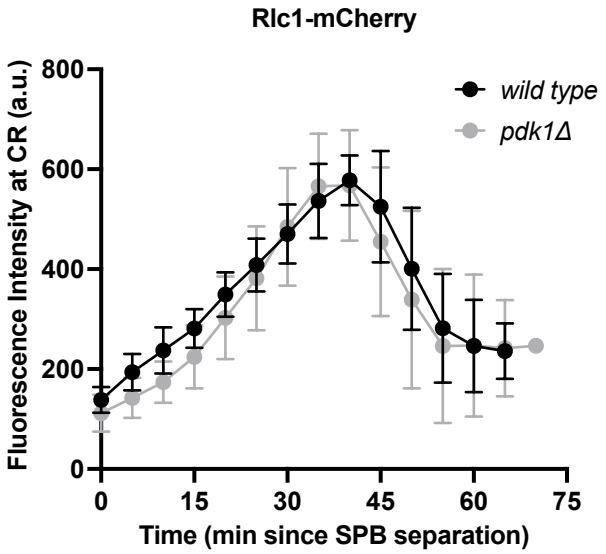
C
Rlc1-mCherry
Fluorescence Intensity at CR (a.u.)
Time (min since SPB separation)
wild type
pdk1Δ
0
200
400
600
800
0
15
30
45
60
75